

Deep UV to NIR space telescopes and exoplanet coronagraphs: a trade study on throughput, polarization, mirror coating options and requirements

Kunjithapatham Balasubramanian, Stuart Shaklan, Amir Give'on, Eric Cady and Luis Marchen
Jet Propulsion Laboratory, California Institute of Technology
4800 Oak Grove drive, Pasadena, CA 91109
kbala@jpl.nasa.gov Tel: 818-393-0258

ABSTRACT

The NASA Exoplanet program and the Cosmic Origins program are exploring technical options to combine the visible to NIR performance requirements of a space coronagraph with the general astrophysics requirements of a space telescope covering the deep UV spectrum. Are there compatible options in terms of mirror coatings and telescope architecture to satisfy both goals? In this paper, we address some of the main concerns, particularly relating to polarization in the visible and throughput in the UV. Telescope architectures employing different coating options compatible with current technology are considered in this trade study.

Keywords: Exoplanet, coronagraph, polarization, off-axis telescope, UV, NIR

1. INTRODUCTION

The recently completed Decadal Survey in astronomy and astrophysics¹ "...highly recommends a modest program of technology development to begin mission trade-off studies, in particular those contrasting coronagraph and star-shade approaches....". An internal coronagraph architecture of modest size and cost may consider a 3.8 m aperture off-axis telescope as shown in the optical layout in figure 1. Achieving better than 10^{10} broad-band suppression of star light in the 2 to 10 λ/D high-contrast dark-hole at the image is extremely challenging. If the telescope is expected to provide adequate throughput from VUV to NIR, additional challenges emerge. Polarization aberration caused by the various mirrors restricts the contrast achievable in such off-axis systems due to the large angles of incidence encountered at the mirrors. We examine here a few options on coating designs that may provide modest contrast performance at a cost of throughput.

1.1 Telescope Architecture

A reference telescope architecture (figure 1) has been proposed² (Shaklan, et al, SPIE 2011) for the exoplanet coronagraph. This employs a 4m diameter primary mirror (PM) with a 3.8 m clear aperture (CA) and a 0.4 m dia secondary mirror (SM). Studies have shown that this is approximately the largest aperture that can be realistically accommodated in existing (e.g. Atlas V) launch fairings.³ An off-axis design is necessary to provide an unobscured aperture for the coronagraph; apertures with a central obscuration require low-throughput Lyot stops that are not suitable for exo-earth imaging.

The separation between the primary and secondary mirrors is 5.5 m (vertex to vertex). The THEIA⁴ Astrophysics Strategic Mission Concept Study (ASMCS) showed that this is the maximum length of the telescope consistent with the fairing length and the stack height required for a wide-field general astrophysics camera⁵, a deep UV spectrometer⁶ and the spacecraft. Table 1 shows the telescope design parameters. In designing the telescope we also considered a Gregorian design but this required a faster primary mirror that would likely have tighter stability tolerances in addition to being more difficult to manufacture.

The coronagraph instrument is based on the ACCESS^{7,8} design. The beam is folded at a flat upstream of the f/24 Cassegrain focus. This is followed by an off-axis parabola (OAP, labeled Tertiary Mirror in fig. 1). A pupil image is formed at deformable mirror DM1, which is then followed by DM2. The sequential arrangement of DMs is used for both phase control and broadband amplitude control.⁹ A second OAP forms an f/21 image where the coronagraph mask is placed. This is followed by a fold mirror and the Lyot Stop. Our contrast modeling includes the primary mirror (PM), secondary mirror (SM), and the optics up to the final OAP before the coronagraph mask. The coronagraph modeling is done with an ideal radial 1-sinc² type focal plane mask followed by a Lyot stop to block diffracted light as discussed in section 5.2.

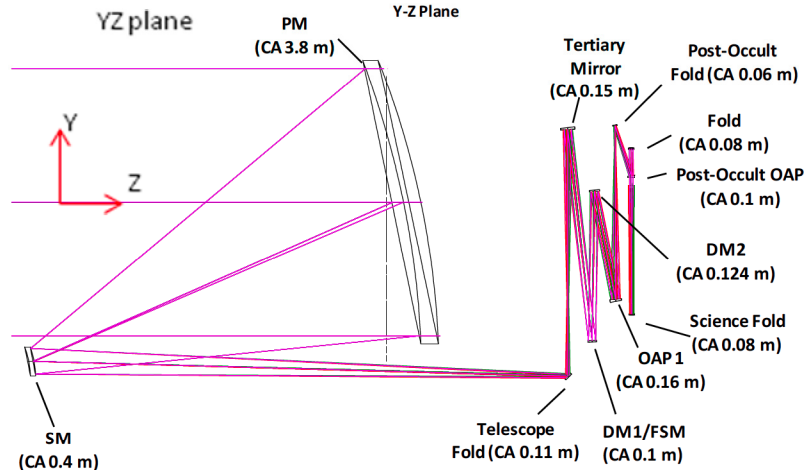


Figure 1. Telescope and instrument layout

1.2 Combining UV and Visible performance requirements

The fast off-axis telescope shown in figure 1 presents large angles of incidence (up to about 21 deg) for rays incident at the PM and SM. The amplitude and phase of reflected light vary strongly with angle of incidence (AOI) and polarization and hence the wavefronts seen by the DM are significantly different for mutually orthogonal polarization states. Secondly, requiring the telescope to provide adequate throughput from VUV to NIR spanning a wavelength region from about 100 nm to 1100 nm presents challenges as listed in Table 2. Mirror coatings are also restricted to a few materials as discussed in the following sections. Coronagraph performance impact due to polarization aberrations due to mirror reflections were examined earlier by Breckinridge, *et al*¹⁰ and Balasubramanian, *et al*¹¹.

Table 1. Telescope Design Parameters

Design	Cassegrain
PM Diam	4 m
PM Clear Ap.	3.8 m
PM-SM separation	5.5 m along Z axis
PM ROC, conic	12.155 m, k=-1
PM Parent f/no	F/0.69
PM Angle of Incidence	2.8-19.9 deg
Off-axis displacement	2.5 m
SM ROC, conic	1.237 m, k=-1.3057

Combined UV telescope + visible coronagraph		
UV preferred state	UV + Coronagraph	Challenge
On-axis telescope	off-axis telescope.	Impacts UV wide-field imaging; very fast parent parabola; More complicated to build and test.
Diffraction-limited performance	Ultra-stable	Very tight requirements on mirror shape and position; Require a complex thermal control system
Deep UV to VUV	Deep UV in addition to Visible and NIR	Compromise UV and/or coronagraph performance.
In this paper, we address only this last point: impact of UV on coronagraph and coronagraph on UV.		
<ul style="list-style-type: none"> Design: 3.8m dia fast off-axis telescope with 5.5m PM to SM separation Polarization splitting and cross polarization coupling due to such design present incoherent orthogonal wavefronts at the coronagraph DM Fitting a non-deployed off-axis telescope and the other back-end instruments into a large rocket fairing allows only about 5.5m mirror separation Coronagraph requires total uncorrected leakage contribution to contrast to be <1e-10 even with fixed patterns from the instrument so that it does not drive the integration time. 		

Table 2. Challenges in combining UV telescope and visible coronagraph

2. HUBBLE TELESCOPE COATING

To obtain light throughput in the VUV region down to about 110nm wavelength, the Hubble telescope primary mirror was coated with aluminum protected by a thin layer of MgF_2 to prevent oxidation and consequent loss of UV photons. Figure 2 shows a theoretical plot of reflectance vs. wavelength at normal incidence for such a mirror assuming optical constants of the materials from literature.

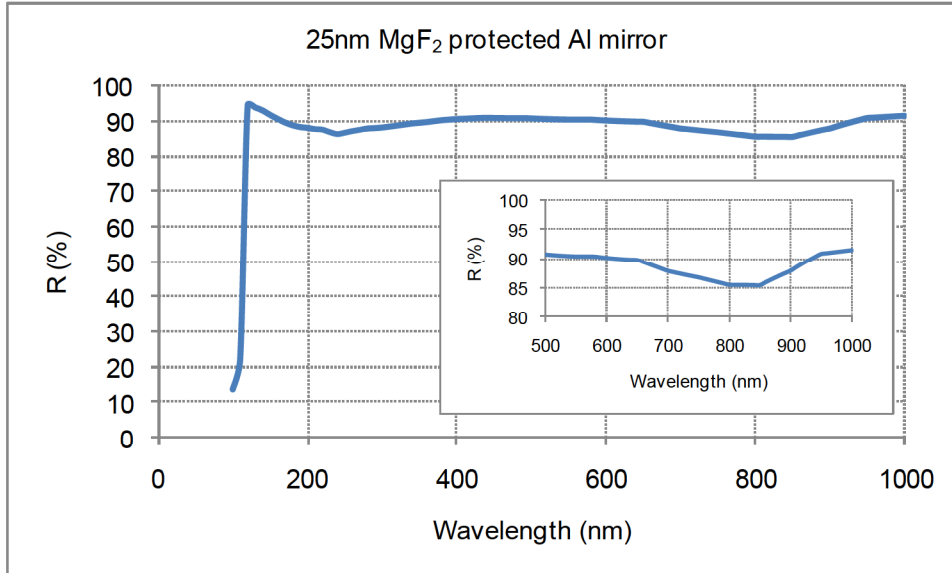


Figure 2. MgF_2 protected Al (theoretical design with optical constants of materials from literature). Note that the reflectivity at the VUV end of the spectrum will depend on the coating process conditions which affect the optical constants of the films.

Aluminum exhibits lower reflectivity than silver and hence throughput of aluminum based systems suffers when the system consists of 3 or more front-end mirrors as is typical of large telescopes. However, aluminum is the only choice for the mirrors if deep UV reflectance is required. Consequently, for a system consisting of 5 mirrors employing protected aluminum as shown in figure 2, the throughput will be only about 60% at 600nm and less than 45% around 800nm. This would be a compromise with aluminum mirrors particularly for a coronagraph aiming to image dim exoplanets. Nevertheless, to combine visible and UV requirements, we need to consider Al based mirrors for the telescope. One could consider using Al for the first 3 mirrors before splitting the light into two channels for the two different missions and then silver for the rest of the mirrors in the system.

3. OBLIQUE RESPONSE AND POLARIZATION

At non-normal incidence, the reflectances of p and s polarizations are different and they suffer a phase difference between them resulting in an elliptical polarization. Figures 3 and 4 show the polarization, defined as $(R_s - R_p)/(R_s + R_p)$, and phase difference between s and p polarizations vs angle of incidence for MgF_2 protected Al mirror. The spectrum of interest to exoplanet coronagraphs is from 400 to 1100 nm while general astrophysics programs expect to reach below 110 nm. Besides throughput requirements, coronagraphy requires tight control of polarization of light in the instrument because the deformable mirror employed for wavefront control and star light suppression can't control two orthogonal incoherent fields with different wavefronts simultaneously to suppress the star light to below 10^{-10} level. Figures 3 and 4 show that a telescope with such mirrors will present two significantly different orthogonal fields over the pupil as illustrated in section 5. Any coating imperfections such as microstructures common to simple vapor deposited coatings may cause additional anisotropic behavior that is not considered in this study which assumes ideal coatings. Advanced coating processes such as reactive sputtering and ion assisted deposition would reduce or eliminate such columnar microstructure of thin films.

4. COATING OPTIONS

The need to cover the full range of wavelengths from about 100nm to 1100nm constrains the number of materials one can consider for optimizing polarization aberrations through coatings. Fluorides such as MgF_2 , LiF , AlF_3 , LaF_3 , Na_3AlF_6 , YbF_3 , CaF_2 , and GdF_3 are candidates to consider. Lower end of this spectrum and expected throughput in that region restrict the choice even further, though mixed materials and multilayers with chosen coating processes to reduce absorption in the UV may offer some advantages.

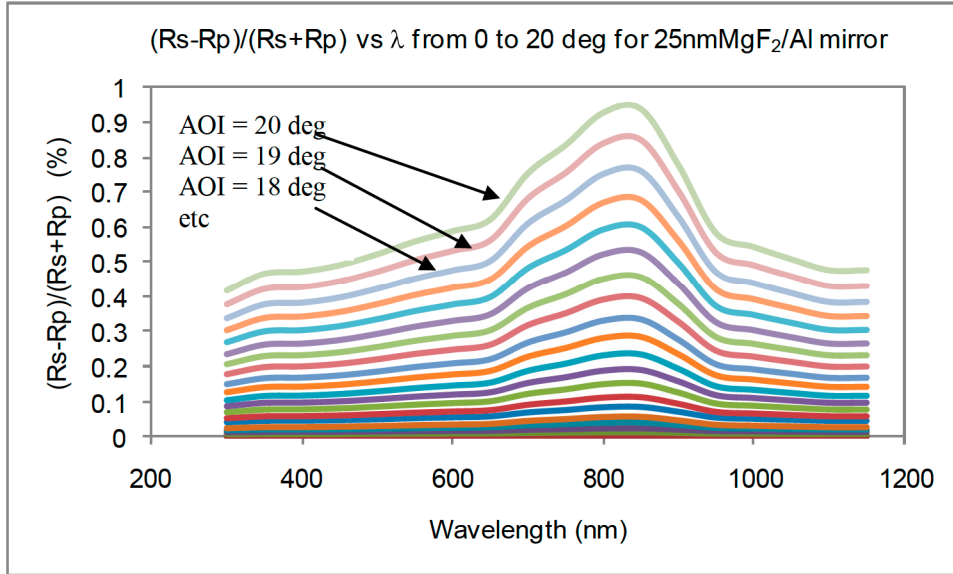


Figure 3. Polarization on reflection from an MgF₂/Al mirror

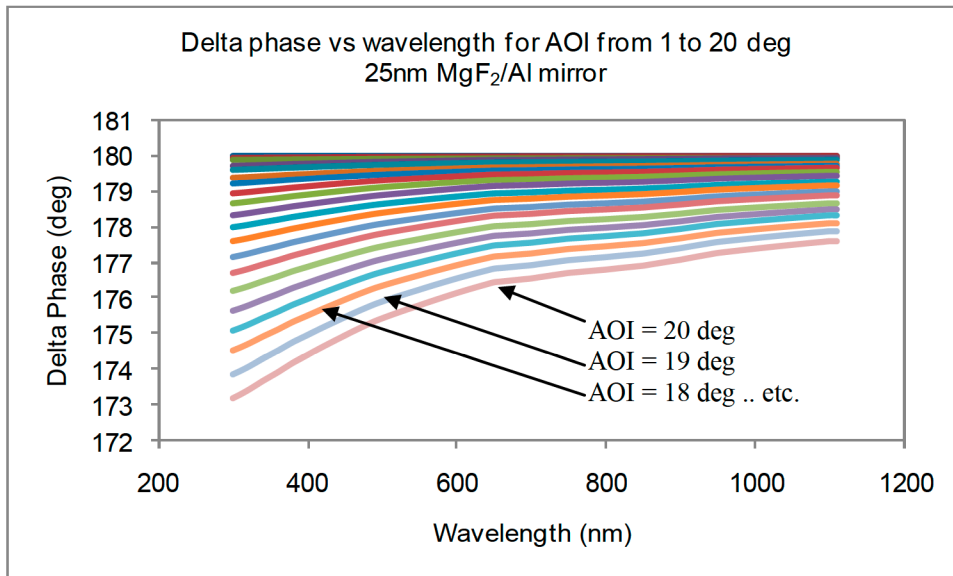


Figure 4. Delta phase between s and p polarization reflected off of 25nm MgF₂ protected aluminum mirror

In this study, we restrict to the use of MgF_2 , LiF , AlF_3 and LaF_3 for protecting Al and optimizing throughput and polarization. Optical constants for all these materials over the full spectrum are not readily available and hence we assembled data from several sources, though such assembled data may be subject to errors. Hence the designs should be considered a guide and not as proven design parameters. Yet they give a reasonable estimate on the achievable performance.

Aluminum needs a protective overcoat to prevent oxidation and consequent absorption in the UV. A thin layer of MgF_2 can provide adequate protection as in the case of Hubble telescope. Similarly, LiF can also protect Al, though its hygroscopic nature requires safeguards during the life of the system, particularly on ground. Besides environmental protection, one needs to consider the optical performance of these coatings. Reducing the phase difference between s and p polarizations as a function of AOI and wavelength is a primary goal in the design and choice of coatings. So also, the amplitude difference between s and p over wavelength and AOI has to be minimized. This must be accomplished with minimum total thickness of the layers to reduce absorption of light in the deep UV. Hence, compromises become necessary unless and until absorption-free coatings are developed.

Bridou *et al*¹², recently studied thin films of MgF_2 and LiF for VUV applications and reported their optical constants in the VUV region. Their studies indicate that MgF_2 can be employed to perform adequately down to about 110 nm if its thickness is less than about 35 nm. LiF can go down to about 100 nm. Similarly, they showed that AlF_3 could be an excellent candidate to go down to about 100 nm. There are spectral lines of interest in that region for astrophysics. Hence we adopted these materials in our designs to study coronagraph performance in the visible.

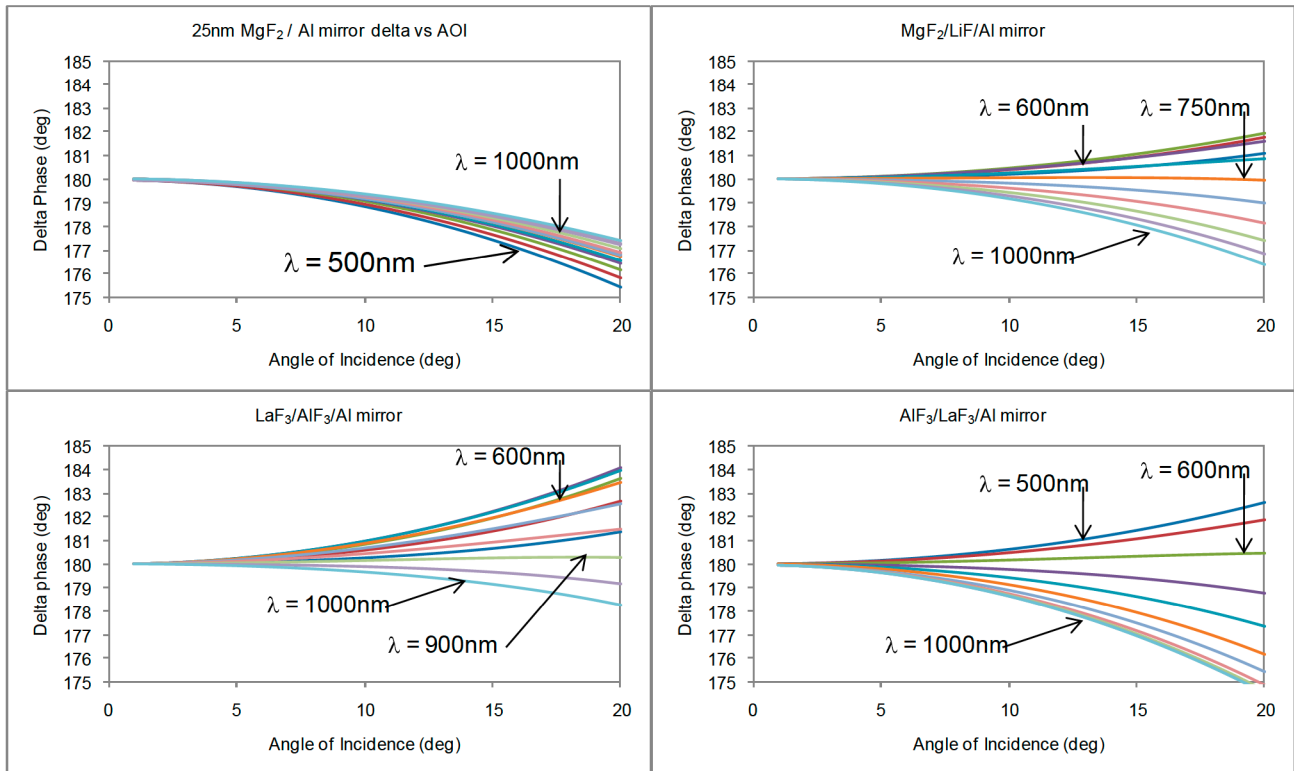


Figure 5. Phase difference between s and p polarizations as a function of AOI for various wavelengths from 500 to 1000 nm for different types of mirror coatings.

Figure 5 shows delta phase vs angles of incidence from 0 to 20 deg for wavelengths ranging from 500 to 1000nm for 4 different coating options. Figure 6 shows the same as a function of wavelength for various angles of incidence from 0 to 20 degrees for the same coatings. The maximum angle of incidence encountered by any ray in the system shown in figure 1 is about 21 deg. Combining these options on various mirrors in the system, one may balance the polarization effects to some extent. As a multi variable problem, optimization is challenging and subject to manufacturing uncertainties as well.

Besides single layer protected Al and Ag mirrors, multilayer options may be attempted to enhance reflectance as well as to reduce polarization splitting. However, these options tend to limit broad band performance as discussed in later sections. UV to NIR reflectance of the various coatings is shown in figures 7a and 7b. Table 3 shows the selected materials and layer structures employed in this study. Throughput to the final image may be optimized by choosing silver based mirrors beyond the split of UV and visible channels.

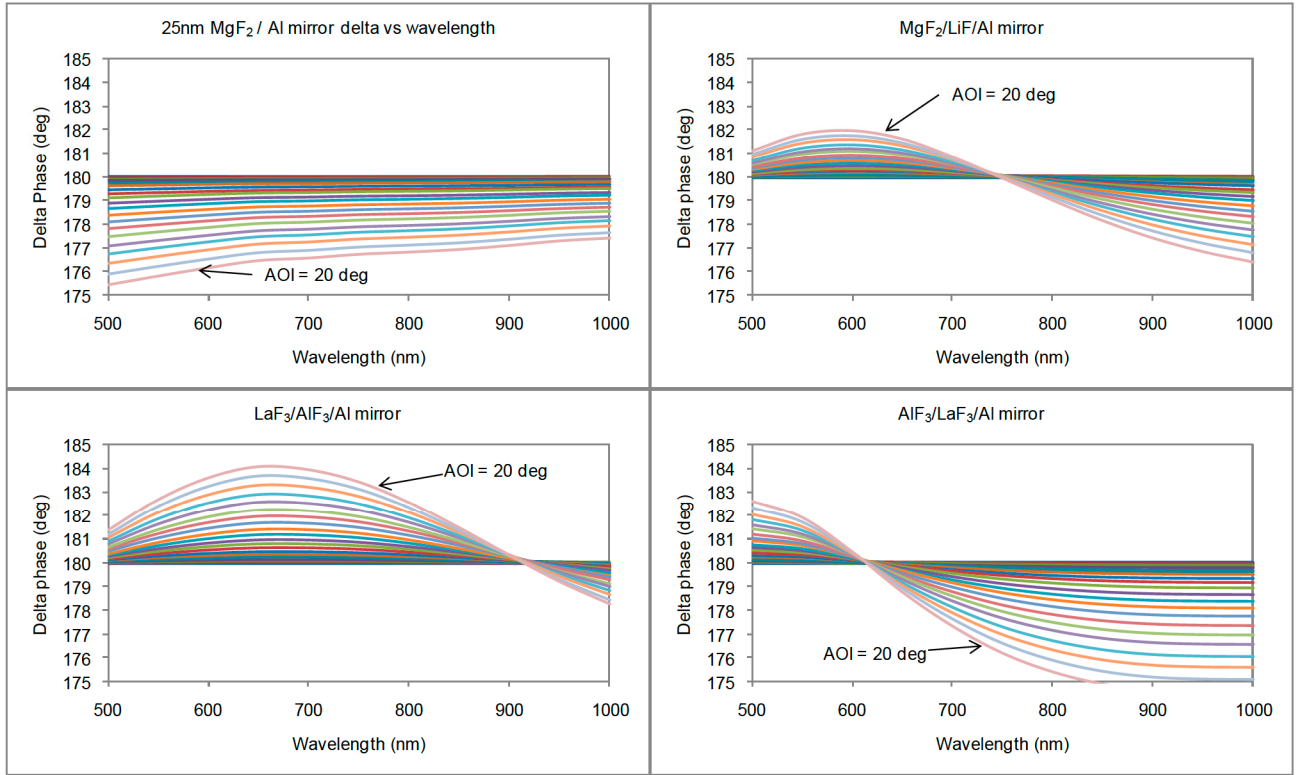
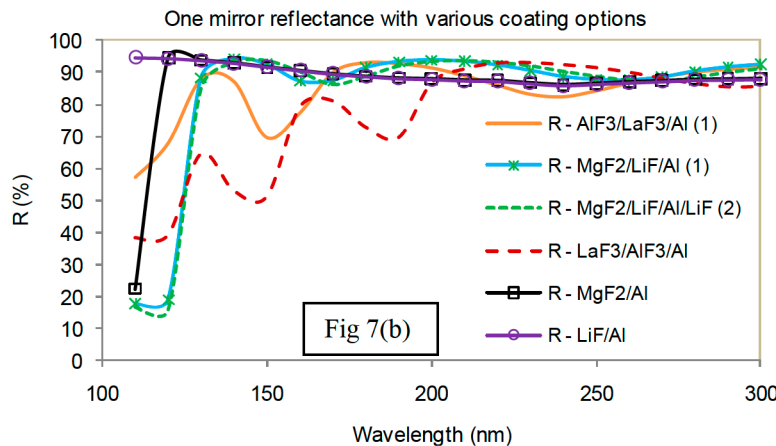
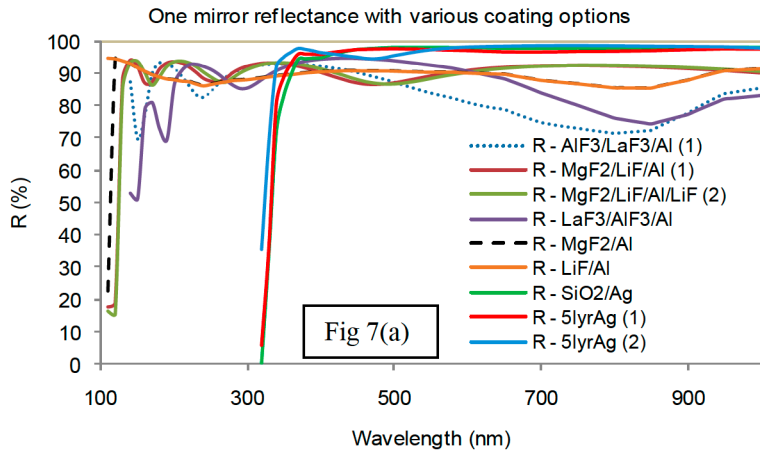


Figure 6. Variation of delta phase between s and p polarizations as a function of wavelength and angle of incidence for various coating options



While figures 2 to 6 show the nature of some candidate coatings and their effects on polarization of reflected light from aluminum mirrors, we discuss the full telescope response in the following sections.

Coating ID	Coating Description
A1	25nmMgF ₂ /Al
A2	10nmMgF ₂ /70nmLiF/Al
A3	5nmMgF ₂ /10nmLiF/Al
B1	Si ₃ N ₄ /SiO ₂ /Si ₃ N ₄ /Al ₂ O ₃ /Ag
B2	Si ₃ N ₄ /SiO ₂ /Si ₃ N ₄ /Al ₂ O ₃ /Ag (B1 w/different thicknesses)
B3	11nmAlF ₃ /87nmLaF ₃ /Al
D	78nmLaF ₃ /58nmAlF ₃ /Al
F	30nmMgF ₂ /110nmLiF/Al
G	55nmMgF ₂ /90nmLiF/Al

Figure 7. (a) R vs λ from 100 to 1000 nm for various mirror coatings (b) R vs λ from 100 to 300 nm for various mirror coatings

5. PUPIL FIELDS WITH DIFFERENT TYPES OF COATINGS ON THE MIRRORS

To simplify the analysis, we launch one polarization into the entrance aperture of the telescope and map the output fields at a relayed pupil, i.e., a DM surface. Polarization aberrations introduced by the telescope mirrors alter the state of polarization of the incident light and render it slightly elliptically polarized with different levels of ellipticity across the pupil.

In general, the total field at the pupil can be described as follows.

$$\text{Total Field } E = A_{xx} e^{i\phi_{xx}} + a_{xy} e^{i\phi_{xy}} + A_{yy} e^{i\phi_{yy}} + a_{yx} e^{i\phi_{yx}} \quad (1)$$

where “A” refers to the main term and “a” refers to the cross term induced in the system due to various reflections.

The subscripts xx refer to the x polarization field at the pupil after all the mirrors for the x field incident at the entrance aperture. The subscripts xy refer to the x field created by incident y field and similarly yx refers to the y field created by incident x field.

5.1 Example: MgF₂/Al mirrors

Figure 8 shows the amplitude and phase maps of Exx and Exy polarizations at the pupil (i.e., DM surface) due to incident x and y polarizations. The cross polarization term Exy, i.e the x field induced by the incident y field will be incoherent with Exx, though both may pass unattenuated through a polarizer aligned to xx.

In principle, the field after perfect correction of the main term at the DM in the x arm of the coronagraph can be written as,

$$1 + \left(\frac{a_{xy}}{A_{xx}} \right) e^{i(\phi_{xy} - \phi_{xx})} \quad (2)$$

where a_{xy}/A_{xx} represents the amplitude perturbation due to the cross polarization term and $\phi_{xy} - \phi_{xx}$ represents the phase perturbation in an otherwise ideally corrected field. The same would be the case for the y polarization arm of the coronagraph. These leakage terms degrade the contrast achievable with the coronagraph.

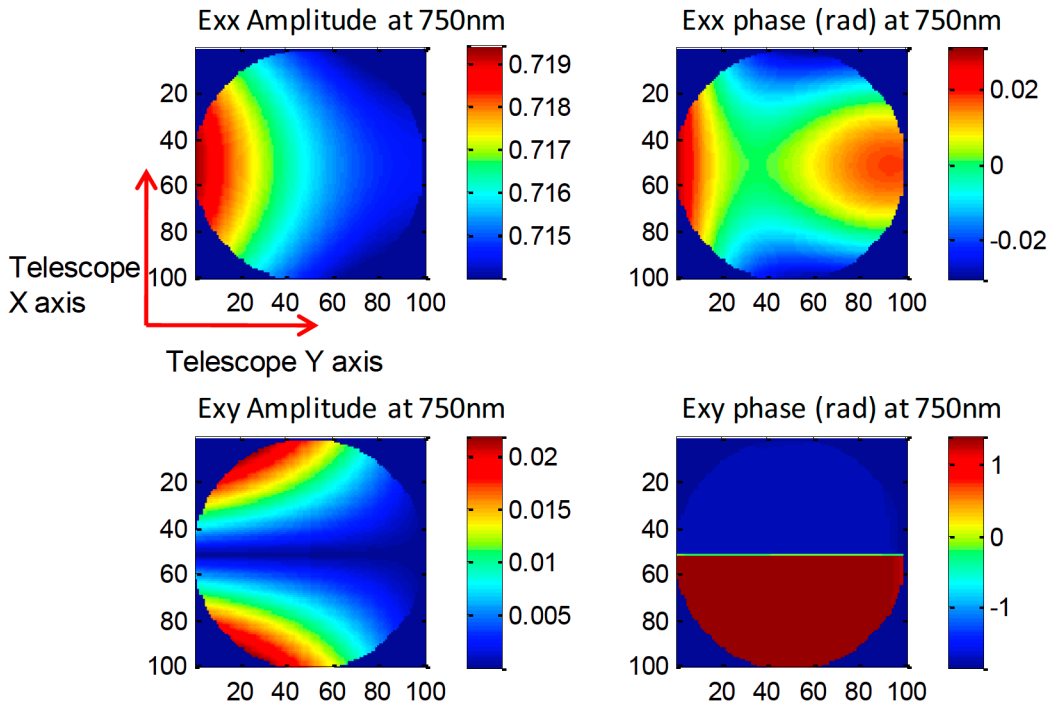


Figure 8. Exx and Exy field pupil maps with the telescope mirrors coated with 25nm MgF₂ protected Al

The xx and xy phase and amplitude maps are significantly different and mutually incoherent. Hence, after DM correction of the xx field, the residual of xy leaves a background light in the image. Though the amplitude of the cross term is only about 2% peak to valley (pv) of the main term, its contribution to the background speckles in the image is significant as it remains largely untouched by the DM. Hence the goal is to find coatings that will reduce the cross term amplitude and phase variation across the pupil, while at the same time not reduce the overall throughput in the visible as well as in the UV.

5.2 Coronagraph performance

The pupil fields obtained with the chosen off-axis telescope architecture and coatings are propagated through an ideal band limited 1-sinc² type circular focal plane mask and a subsequent Lyot stop to block the diffracted light. The images formed at the final image plane are analyzed for contrast at a chosen rectangular region. Employing Electric Field Conjugation (EFC) algorithm¹³ (Give'on, 2009), a dark hole is created in the rectangular region covered by 2 to 5 λ/D and -5 to 5 λ/D at the final image. Figure 9 shows the field maps and corresponding final image with the dark hole region for Case A (all mirrors with 25nm MgF₂ protected Al) of the telescope design.

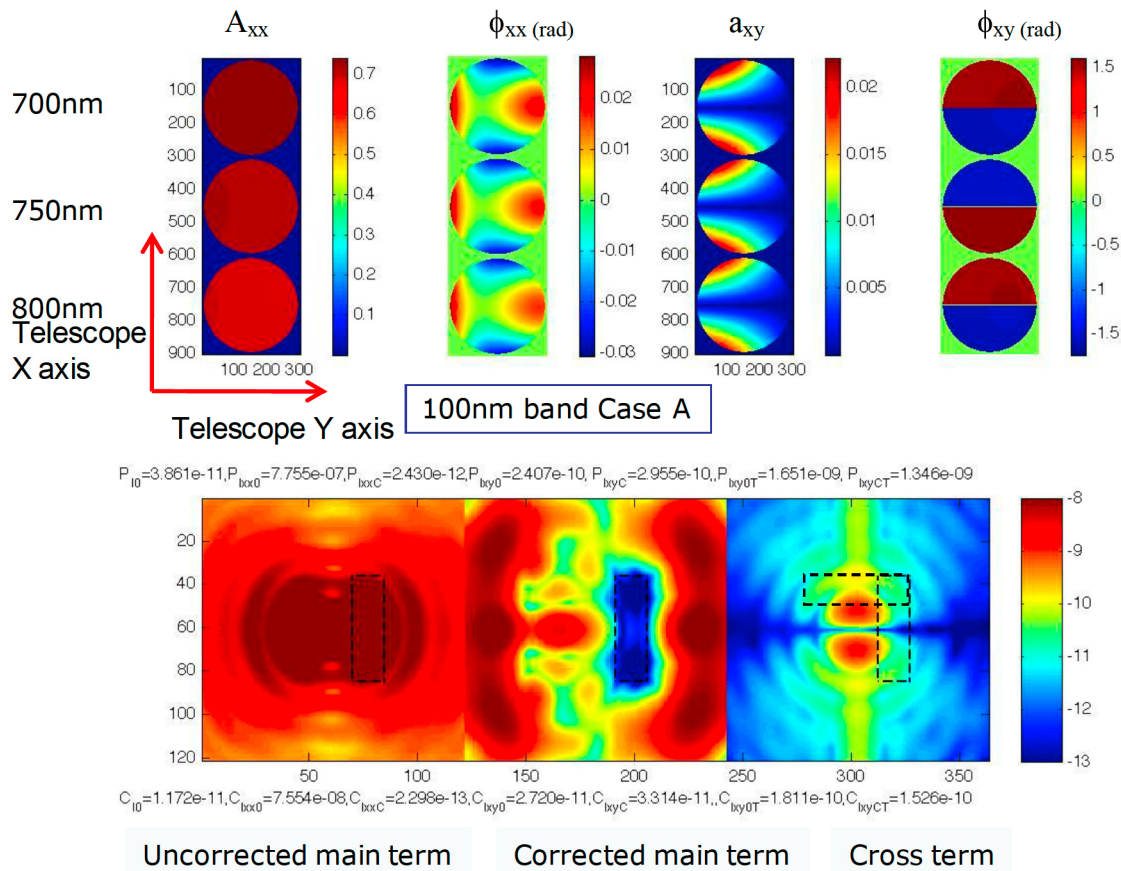


Figure 9. Contrast in the dark hole in the image due to the main and cross term field for the system of mirrors coated with 25nm MgF₂/Al. The upper panel shows field amplitude and phase maps for xx and xy polarization terms (as defined in equation 1, section 5) for 700, 750 and 800nm wavelengths. The lower panel shows the corresponding images of uncorrected xx, corrected xx and uncorrectable xy terms after passing through the focal plane mask and Lyot stop. The dotted lines show the rectangular boxed region [2,5,-5,5 λ/D] of dark hole in two orientations.

Note that in figure 9, the dark hole is generated in the axis where scattered light due to the cross polarization term is less. This is the axis orthogonal to the axis of symmetry in the telescope. Average and peak values of the contrast in the boxed region are shown by C_{IxxC} , P_{IxxC} , etc. C_{IxyCT} is average contrast in the upper boxed region of xy term image where the contrast is poor; “T” signifies transposed region.

5.3 MgF₂/LiF protected Al mirrors

Lithium fluoride has roughly the same refractive index as magnesium fluoride in the visible spectrum, but has a lower absorption in the VUV region. Therefore, employing a layer of LiF to protect Al from oxidation is an option¹⁴. However, due to the hygroscopic nature of LiF, another layer is needed to protect LiF. One may employ a thin layer of MgF₂ or AlF₃ for this purpose. Different combinations of such layer schemes may provide a path for optimum system performance. The peak to valley and spatial variation of the amplitude and phase of the cross polarization term across the pupil differ by factors of 2 to 10 depending on the nature and application of these coatings. They are also wavelength dependent.

5.4 Other coating options and their performance

Double layer coatings employing AlF₃ and LaF₃ also provide better performance for the coronagraph than a single thin layer of MgF₂ on Al. However, the VUV reflectivity of these coatings is <50% in the 110 to 120 nm band and hence the throughput after 3 reflections will be only ~ 10 to 15%. The telescope throughput in the visible spectrum is about 50% depending on the wavelength because Al reflectivity is low. Detailed experimental investigations are therefore necessary to determine the throughput and cut off wavelength as the optical constants could vary depending on the coating process employed. DUV and VUV material properties are discussed by Thielsch¹⁵ in Kaiser & Pulker (2003). A recent study of LaF₃ and AlF₃ thin films was reported by Xue¹⁶ and Shao (2010).

Table 4 lists the various cases studied here with different coating options on different mirrors in the system. Cases A, B, C, D and E are evaluated for contrast by passing the respective fields through the coronagraph with the DM correcting the phase and amplitudes in broadband from 700 to 800 nm bandwidth. We include the case of silver based system (Case B) here for comparison, though silver has no throughput for deep UV astrophysics. Field maps with Cases J and K are examined for amplitudes and phases of cross terms. These are roughly similar to Case A. The Case K (thinner layers) is likely to perform marginally better for throughput and contrast.

Table 4. Different cases of coatings on the telescope mirrors					
Cases Studied	PM	SM	3rd OAP	Approximate cut -off λ	average visible T through 5 mirrors
Case A	A1	A1	A1	110 to 120nm	52%
Case B	B1	B2	B2	350 to 400nm	92%
Case C	F	G	A	120 to 150nm	49%
Case D	B3	D	D	120 to 150nm	39%
Case E	F	F	F	120 to 150nm	39%
Case J	A2	A2	A2	110 to 120nm	38%
Case K	A3	A3	A3	100 to 120nm	53%

Examining the field amplitude and phase maps at the DM surface for the main term (xx) and the cross term (xy) and estimating the mean, peak-to-valley (pv) and standard deviation (stdev) of these fields across the pupil give a guidance on the choice of coatings and their effectiveness. Figure 10 shows the mean, pv and stdev of amplitude with various coating choices for the main term xx and cross term xy at the DM1 surface in the telescope. Figure 11 shows the pv and stdev of the phase of the main term and cross term. Note that the phase swings of the cross term at some wavelengths for some of these cases are a result of π phase jumps that occur where cross term amplitude goes to zero as seen in the phase maps. These figures together with the field maps and contrast results shown in the next section reveal that while minimizing the cross term amplitude reduces the uncontrolled scattered light in the final image, broad band contrast favors a roughly inverse linear dependence of the cross term amplitude and phase with wavelength and hence simple thin MgF₂ protected aluminum mirrors tend to perform adequately, though with some compromises in throughput and discovery space.

6. CONTRAST SIMULATIONS AND RESULTS

As discussed in section 5.2 for the case of MgF_2 protected Al mirrors in the telescope, three other cases of coatings were studied for coronagraph performance. Cases A, B, C and D as listed in table 4 were examined for broadband (100 nm band width around 750 nm) contrast performance with xx term and xy term at the DM surface assuming a perfect polarizer separating the yy and yx terms for an independent channel. Figures 12 to 14 show the amplitude and phase fronts at the pupil on the top panels of each figure and show the final images with dark holes marked by dotted line boxes. The average and peak values of the contrast in these are estimated. In each case, one can see that the cross terms scatter light preferentially in one direction where the contrast will be poor. Hence the discovery space is limited in this coronagraph system mainly due to the nature of scattering in the image due to the cross polarization term. The basic geometry of the telescope system is the driving factor for the cross polarization leakage. This potentially static background may be subtracted when multiple images are captured with rotated orientations and thus a real planet in the image may be extracted. This would result in an overhead on observation time. Regardless, the IWA may be limited by the excessive peak intensity seen at or near $2\lambda/D$.

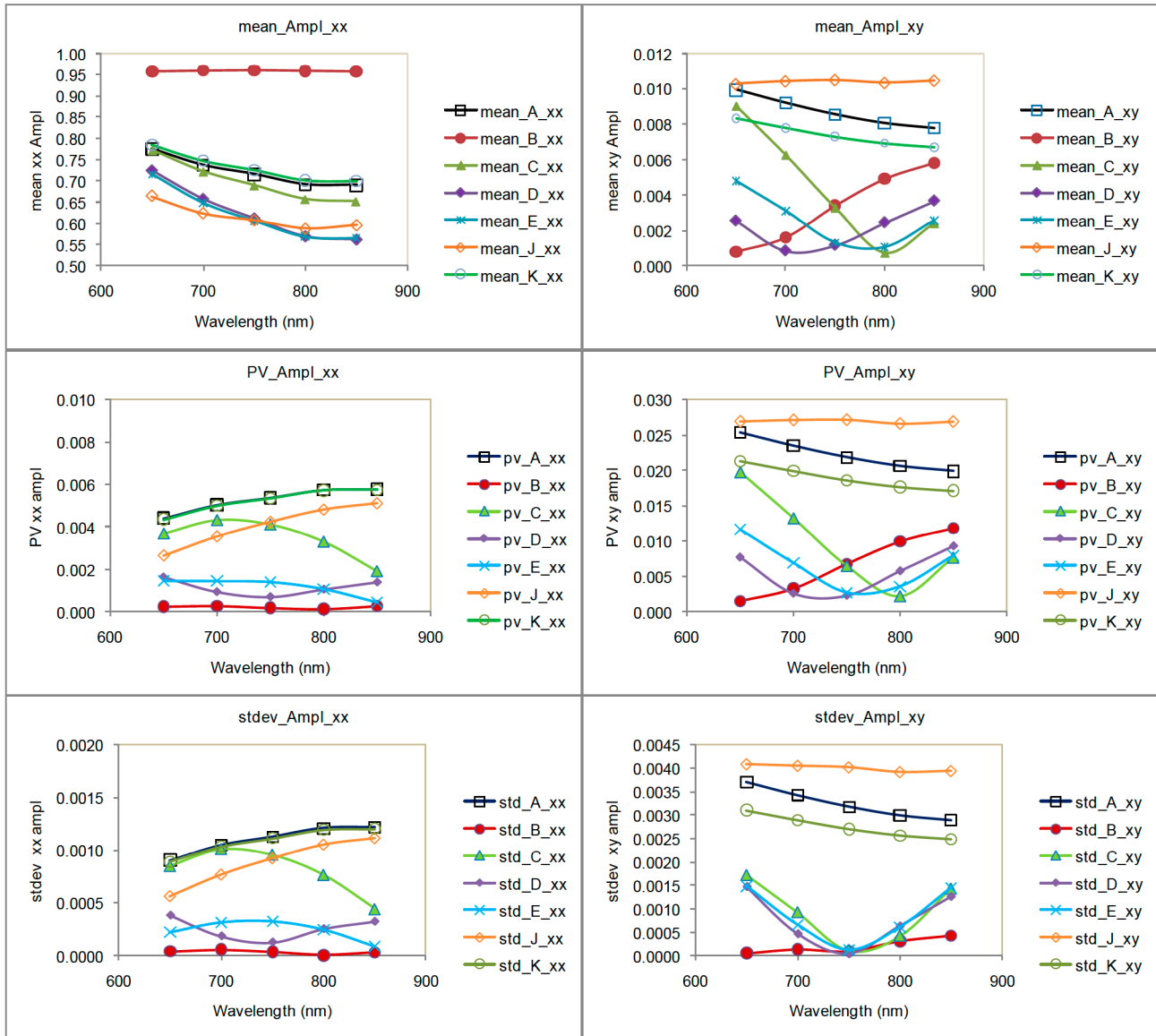


Figure 10. Mean amplitude, peak-to-valley and standard deviation of the main term xx and the cross term xy across the pupil (i.e., DM surface) for different cases of coatings listed in table 4

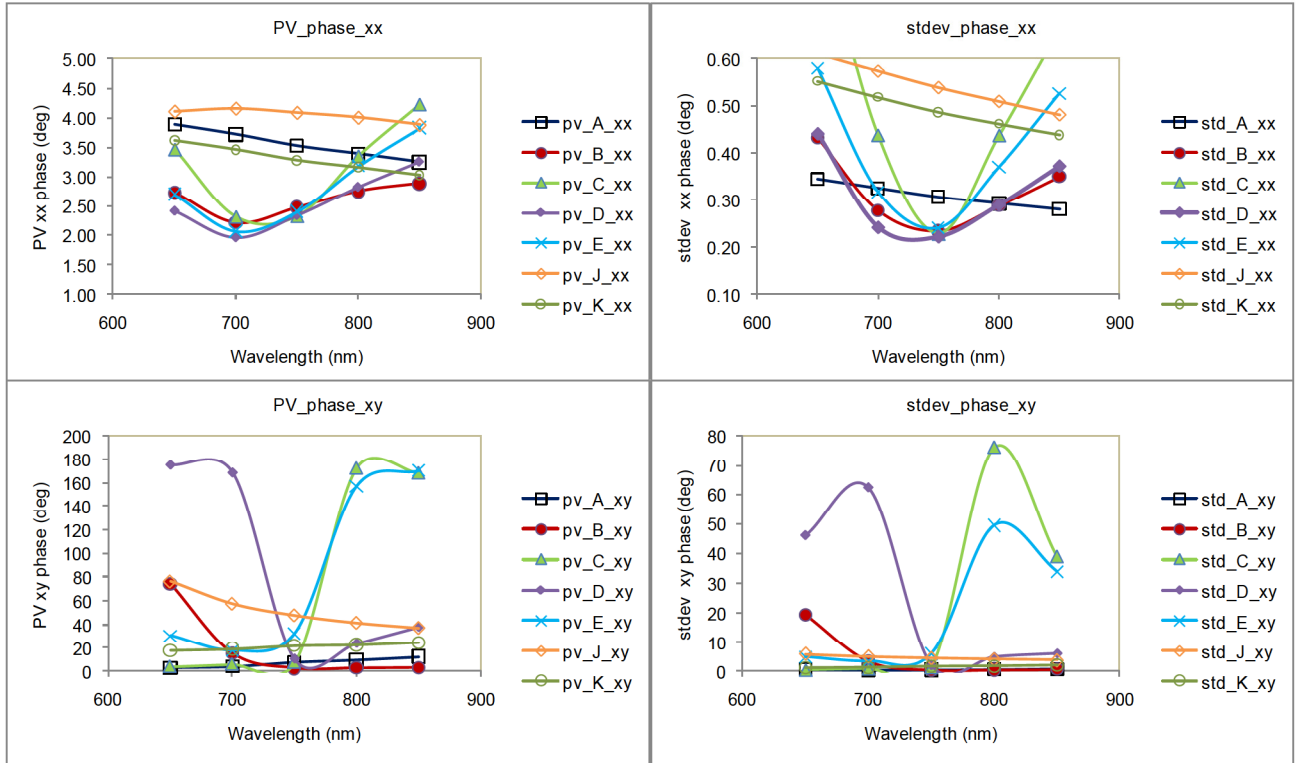


Figure 11. peak-to-valley and standard deviation of the phase of main term xx and the cross term xy across the pupil (i.e., DM surface) for different cases of coatings listed in table 4

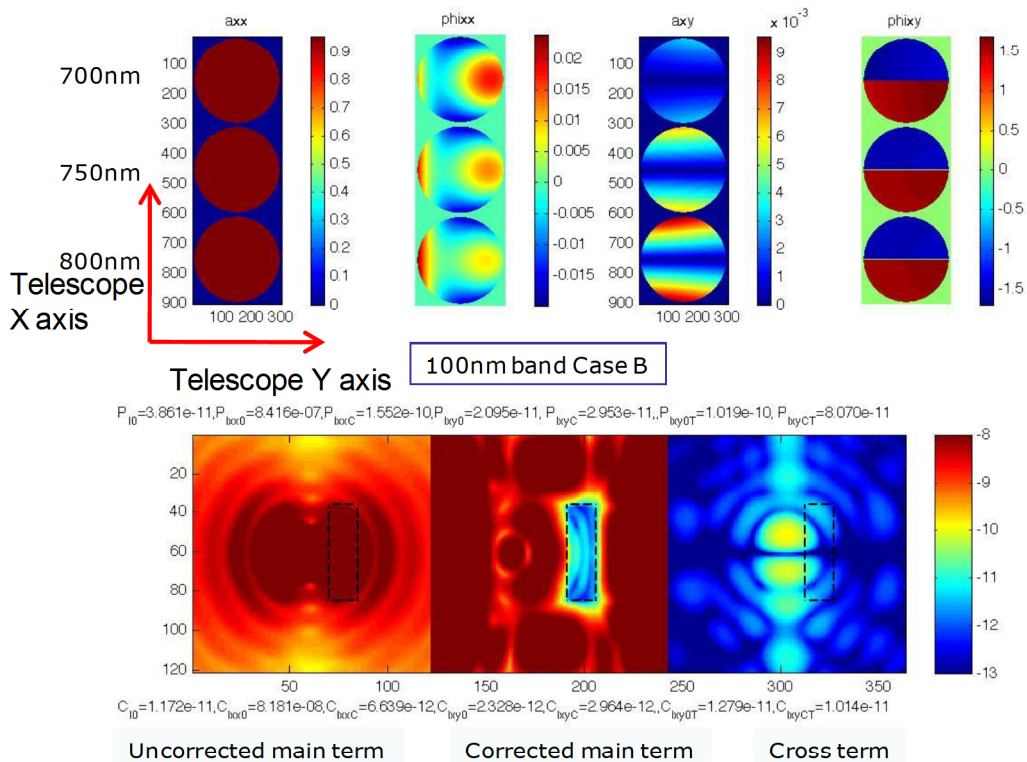


Figure 12. Case B. System with protected Silver based mirrors per tables 3 and 4

7. SUMMARY & CONCLUSIONS

The amplitude of the cross term and its distribution over the pupil largely determine the nature and magnitude of background scatter in the image and hence the achievable contrast in the dark hole region. This cross term arises primarily due to the system geometry. Mirror coatings may increase or mitigate the cross term. Coating non uniformity and anisotropy due to potential columnar microstructures (not included in this study), typical of simple thermal evaporation processes, may also add to the background scatter. Case B with silver based mirrors is better than the rest of the cases for cross term scatter; however, it is not an acceptable option because it has no UV throughput. Case D is reasonably acceptable for coronagraphy though broad band contrast due to the main term is rather poor. The bar graphs in Figure 15 show the relative performance of these cases. Contributions to contrast from the main term and cross term are shown by the different colors. Likewise, the peak values of contrast inside the dark hole are also shown. Case A coating and similar thinner coatings with MgF_2 and LiF (e.g., case K) are likely to be better options for throughput in UV and coronagraph contrast in the visible. In summary,

- Two coronagraph channels are needed for the two orthogonal polarizations. Such a choice would also help with characterizing polarization signals from planets.
- Within one polarization channel, the cross polarization leakage term is not controllable by the DMs. It has unacceptable leakage in the X direction (in the transposed region orthogonal to the PM-SM separation). Hence, an efficient full annular dark hole with $2\lambda/D$ IWA can't be achieved. Discovery space is thus limited.
- $Al+MgF_2$ has the best direct term and the worst cross term. But, the cross term is only a factor of 2 or 3 above the requirement in a small (but important) region. Further optimization may be feasible.
- Case D is the only Al based system with cross-term leakage below our requirements. But this may come at the expense of VUV performance (~ 120 nm cutoff; all process dependent material properties have to be confirmed by detailed experiments).
- Extending the telescope to reduce the off-axis angle will open up the useable region of the dark hole.
- The off-axis configuration studied here is probably acceptable with a simple Al + thin layer of MgF_2 and/or LiF on the mirrors. This will have the best broadband performance (important for reducing sensitivity to aberrations), though with reduced visible throughput. Part of the image plane will not be useable for coronagraphy.

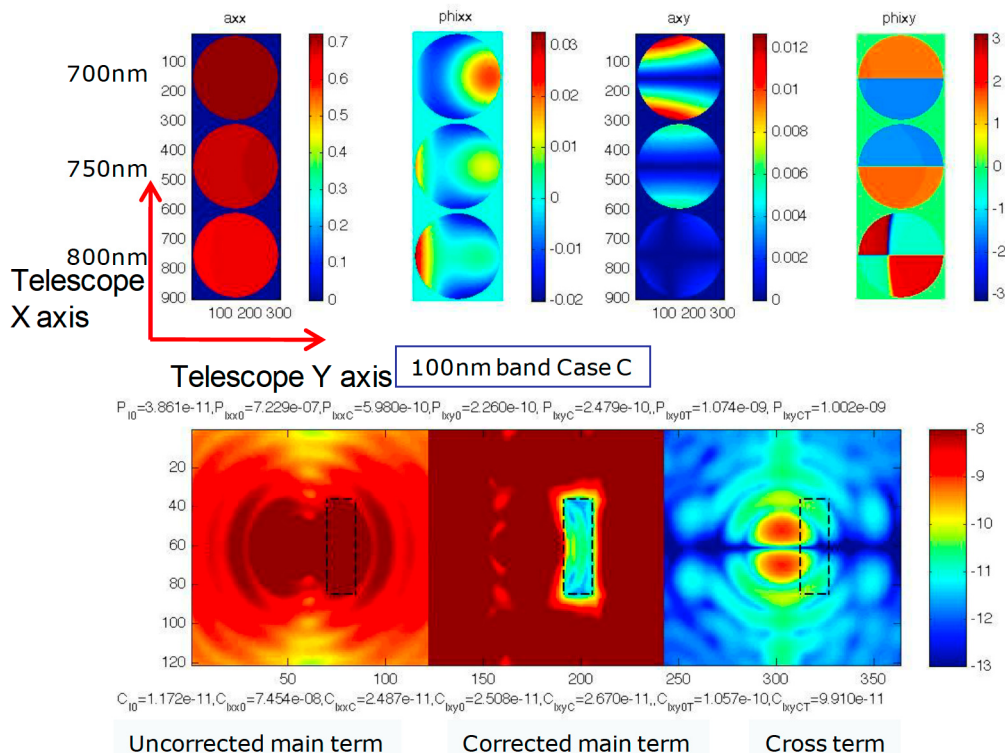


Figure 13. Case C. System with LiF/MgF_2 protected Al mirrors per tables 3 and 4

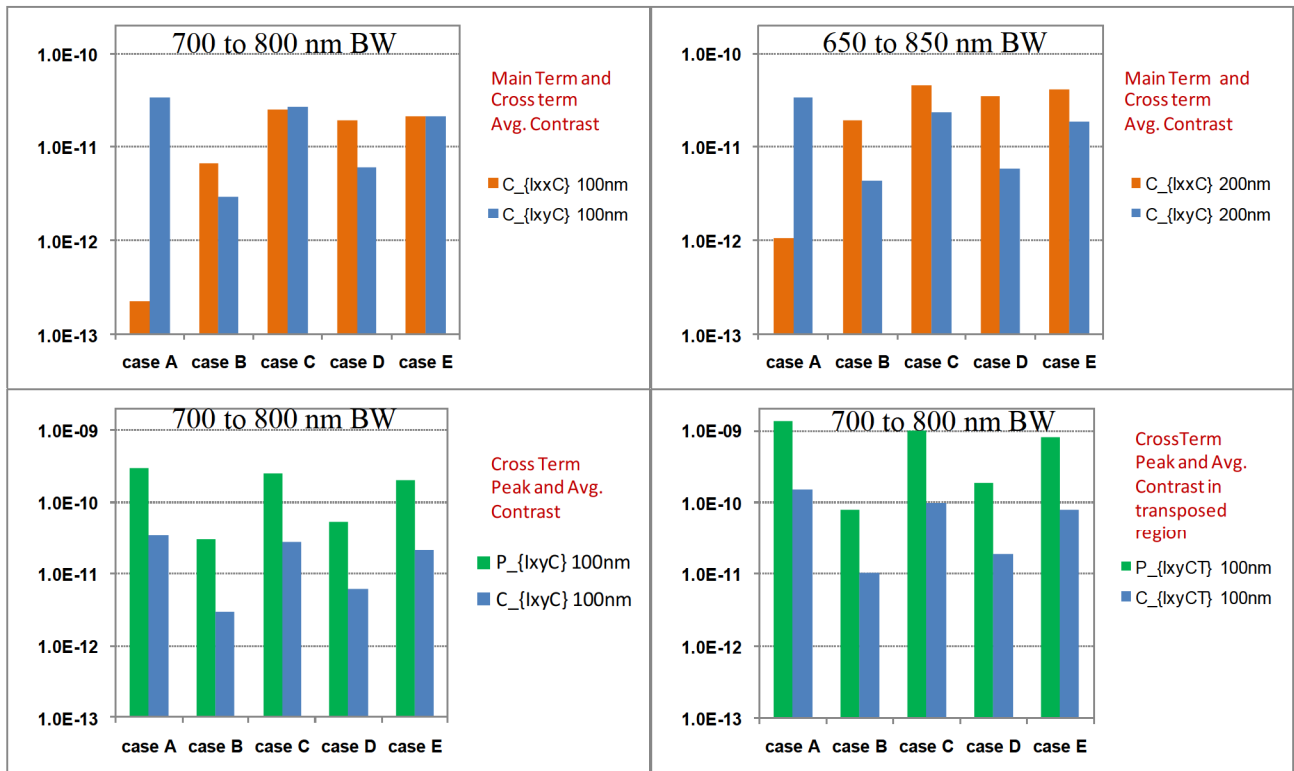
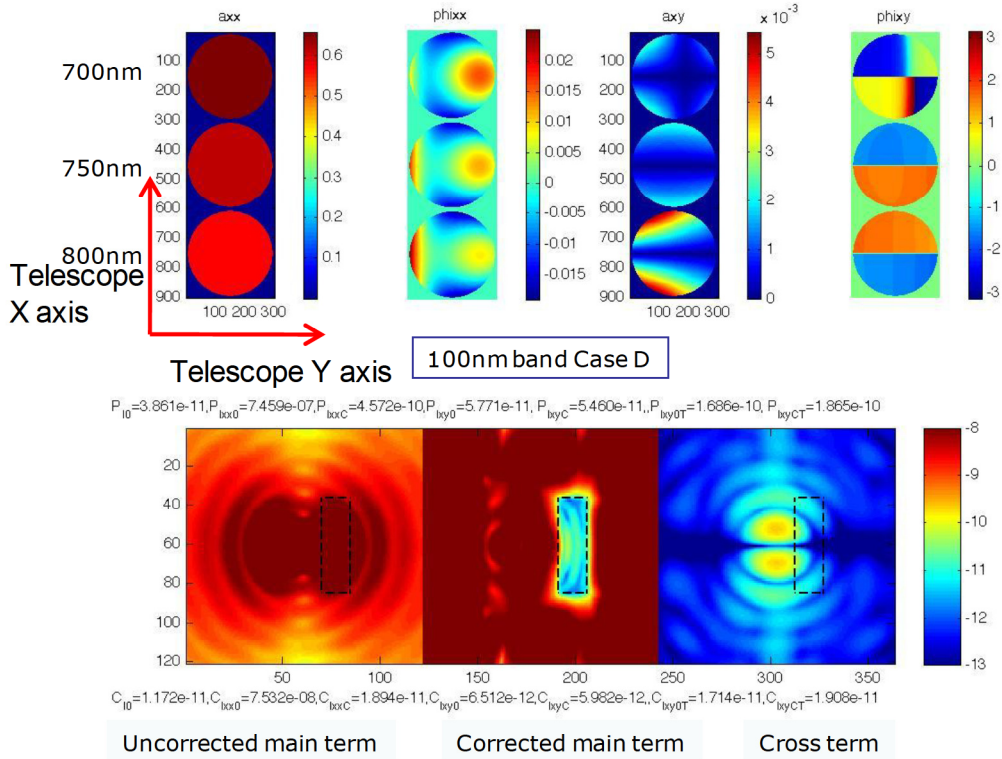


Figure 15. Average and peak contrasts in the dark hole region for various cases examined

8. ACKNOWLEDGMENTS

This work was performed at the Jet Propulsion Laboratory, California Institute of Technology, under a contract with the National Aeronautics and Space Administration.

REFERENCES

- [1] Committee for a Decadal Survey of Astronomy and Astrophysics; National Research Council, "New Worlds, New Horizons in Astronomy and Astrophysics," ISBN: 0-309-15800-1 (2010).
- [2] Shaklan, S. B., *et al.*, Stability error budget for an aggressive coronagraph on a 3.8 m telescope, Proc. SPIE vol. 8151, (in this conference), (2011).
- [3] Shaklan, S. B., *et al.*, "Terrestrial Planet Finder Coronagraph (TPF-C) White Paper for the NASA-NSF Exoplanet Task Force," available at <http://exoplanets.jpl.nasa.gov/documents/TPFC-WhitePaper2-shaklan.pdf> (2007).
- [4] Spergel, D. N. (PI), THEIA ASMCS Documentation, available at <http://www.astro.princeton.edu/~dns/theia.html> (2009).
- [5] Scowen, P. A., *et al.*, "Design and implementation of the NUV/optical widefield Star Formation Camera for the Theia Observatory," Proc. SPIE 7731, 77314Y (2010).
- [6] Kasdin, N. J., "THEIA Telescope for Habitable Exoplanets and Interstellar/Intergalactic Astronomy," White Paper submitted to NRC ASTRO-2010 Survey, available at http://www.astro.princeton.edu/~dns/Theia/nas_theia_v14.pdf (2010).
- [7] Trauger, J., *et al.*, "ACCESS – a NASA mission concept study of an Actively-Corrected Coronagraph for Exoplanet System Studies," Proc. SPIE 7010, 701029-1 (2008).
- [8] Guyon, O., *et al.*, "The pupil mapping exoplanet coronagraphic observer (PECO)," Proc. SPIE 7731, 773129 (2010).
- [9] Shaklan, S. B., & Green, J. J., "Reflectivity and optical surface height requirements in a broadband coronagraph. 1. Contrast floor due to controllable spatial frequencies," Appl. Opt 45, 5143-5153 (2006).
- [10] Breckinridge, J. B. and B. R. Oppenheimer "Polarization effects in reflecting coronagraphs for white-light applications in astronomy", *Astrophys. J.* 600: 1091-1098, (2004).
- [11] Balasubramanian, K., *et al.*, "Polarization compensating protective coatings for TPF-Coronagraph optics to control contrast degrading cross polarization leakage", Proc. SPIE vol. 5905, (2005).
- [12] Bridou, F., *et al.*, "Experimental determination of optical constants of MgF₂ and AlF₃ thin films in the vacuum ultraviolet wavelength region (60–124 nm), and its application to optical designs", *Opt. Communications*, 283 1351-1358 (2010)
- [13] Give'on, A., "A unified formalism for high contrast imaging correction algorithms," Proc. SPIE, vol. 7440 74400D-1 (2009).
- [14] Oliveira, C., *et al.*, "Aging Studies of LiF Coated Optics for Use in the Far Ultraviolet," Proc. SPIE, vol. 3765, (1999). <http://fuse.pha.jhu.edu/papers/technical/spie3765/spie3765-66.pdf>
- [15] Thielsch, R. "Optical Coatings for DUV/VUV", Chapter in *Optical Interference Coatings*, Ed: Kaiser & Pulker, 2003, Springer Series in Optical Sciences, (2003).
- [16] Xue, C., and Shao, J., "Properties of AlF₃ and LaF₃ films at 193nm", Proc. of SPIE Vol. 7655 76553G-1 (2010).